Revisiting the ABC flow dynamo

Ismaël Bouya[1, a)] and Emmanuel Dormy[2, b)]

[1)] *UMR 7586 Institut de mathématiques de Jussieu – Analyse fonctionnelle*

[2)] *MAG (ENS/IPGP), LRA, Département de Physique,*
Ecole Normale Supérieure, 24, rue Lhomond, 75231 Paris Cedex 05,
France.

(Dated: 30 November 2019)

The ABC flow is a prototype for fast dynamo action, essential to the origin of magnetic field in large astrophysical objects. Probably the most studied configuration is the classical 1 : 1 : 1 flow. We investigate its dynamo properties varying the magnetic Reynolds number Rm. We identify two kinks in the growth rate, which correspond respectively to an eigenvalue crossing and to an eigenvalue coalescence. The dominant eigenvalue becomes purely real for a finite value of the control parameter. Finally we show that even for Rm = 25000, the dominant eigenvalue has not yet reached an asymptotic behaviour. It still varies very significantly with the controlling parameter. Even at these very large values of Rm the fast dynamo property of this flow cannot yet be established.

[a)]Electronic mail: ismael.bouya@normalesup.org; http://nsup.org/~bouya/

[b)]Electronic mail: dormy@phys.ens.fr

I. INTRODUCTION

We investigate the kinematic dynamo action associated with the well known ABC-flow (Arnol'd, Beltrami, Childress[1]). We focus on the highly symmetric, and most classical setup: $A:B:C = 1:1:1$. Its dynamo properties have been assessed in 1981 by Arnol'd *et al.*[2] and it represents since then the prototype flow for fast dynamo action. A "fast dynamo"[3] is a flow which achieves exponential magnetic field amplification over a typical time related to the advective timescale and not the ohmic diffusive timescale (in which case it is referred to as a "slow dynamo"). It is known[4] that exponential stretching of fluid elements is necessary for fast dynamo action. The existence of fast dynamos is essential to account for the presence of magnetic field in astrophysical bodies, for which the ohmic diffusive time is often larger than the age of their formation. If self-excited dynamo action is to generate their magnetic fields, it is therefore essential that it be achieved over an advective timescale. The most classical flow to exemplify such "fast dynamo" action is indeed the ABC-flow. Arnold and Korkina[5] first investigated the dynamo property of the ABC-flow, originally introduced to investigate Lagrangian chaos. Many developments followed, which will be discussed in the course of this article[6–8].

Most of the recent developments in this field involve non-linear studies with forcing belonging to the class of ABC flows[9,10], with a few noticeable exceptions[11,12]. The asymptotic behaviour of one of the most classical example of fast dynamo is however still not understood. This motivates the following high-resolution linear study.

II. NUMERICAL METHOD

We are concerned with the kinematic dynamo problem, for which a solenoidal magnetic field evolution is governed under a prescribed flow by the induction equation

$$\frac{\partial \mathbf{B}}{\partial t} = \boldsymbol{\nabla} \times \left(\mathbf{u} \times \mathbf{B} - \mathrm{Rm}^{-1} \boldsymbol{\nabla} \times \mathbf{B} \right) . \tag{1}$$

We consider here the ABC-flow (Arnold[13], Henon[14]), which takes the form

$$\mathbf{u} = (A \sin z + C \cos y)\, \mathbf{e}_x + (B \sin x + A \cos z)\, \mathbf{e}_y + (C \sin y + B \cos x)\, \mathbf{e}_z \,, \tag{2}$$

and restrict our attention to the case where the magnetic field has the same periodicity as the flow (i.e. 2π-periodic in all directions of space, see Archontis, Dorch, and Nordlund[15]

for extensions) and the weight of the three symmetric Beltrami components are of equal strength ($A = B = C \equiv 1$).

Let us stress again that we also restrict our attention to the kinematic dynamo problem, in which the flow is analytically prescribed and unaltered by the magnetic field (see Galloway and Frisch [8] for an investigation of the stability of this flow).

The choice $A\!:\!B\!:\!C = 1\!:\!1\!:\!1$ belongs to the largest symmetry class for this kind of flows, and has for this reason been the most intensively studied. However, it yields very small chaotic regions and is thus possibly non optimal for dynamo action (see Alexakis [11] for a detailed study of this point). This parameter choice is however essential as it is, partly for historical reasons, the most classical example of steady analytical fast dynamo.

The simulations presented in this article were performed using a modified version of a code originally developed by Galloway and Frisch [6] and which uses a fully spectral method with explicit mode coupling.

The original time-stepping used by Galloway and Frisch [6] relies on a Leapfrog scheme stabilised by a Dufort-Frankel discretization of the diffusive term. Introducing $\mathcal{L}$ to denote the discretized diffusion operator, which is local in Fourier space, and $\mathcal{NL}$ to denote the discretized inductive term, non-local as it couples neighbouring modes, this scheme can be expressed as

$$\mathbf{B}^{n+1} = \mathbf{B}^{n-1} + 2\mathrm{d}t \left(\mathcal{NL}(\mathbf{B}^n) + \frac{1}{2}\mathcal{L}(\mathbf{B}^{n+1} + \mathbf{B}^{n-1}) \right) , \tag{3}$$

using a red-black (or Chloride-Sodium) staggering in time and space, see Galloway and Frisch [7].

We have implemented two alternative time stepping schemes, in order to assess the stability of the temporal evolution at large values of Rm. We used a Crank-Nicolson Adams-Bashforth scheme

$$\mathbf{B}^{n+1} = \mathbf{B}^n + \mathrm{d}t \left(\frac{1}{2}\mathcal{L}(\mathbf{B}^{n+1} + \mathbf{B}^n) + \frac{3}{2}\mathcal{NL}(\mathbf{B}^n) - \frac{1}{2}\mathcal{NL}(\mathbf{B}^{n-1}) \right) , \tag{4}$$

as well as a second order BDF discretization

$$\frac{3}{2}\mathbf{B}^{n+1} = 2\,\mathbf{B}^n - \frac{1}{2}\,\mathbf{B}^{n-1} + \mathrm{d}t \left(\mathcal{L}(\mathbf{B}^{n+1}) + 2\,\mathcal{NL}(\mathbf{B}^n) - \mathcal{NL}(\mathbf{B}^{n-1}) \right) . \tag{5}$$

These two schemes are unstaggered and involve larger memory requirements, still offering the same complexity. All schemes are semi-implicit, but retain an explicit marching for the

non-local term in order to prevent the resolution of a linear system at each time-step. We verified that the results presented in this article are independent of the above choices.

In the limit of large magnetic Reynolds numbers, the problem (1) becomes stiff. We therefore ensured that the temporal discretization did not introduce spurious effects by reproducing a few simulations, spanning over the whole range of Rm investigated, using the three schemes presented above.

We always obtained the same dominant mode and temporal behaviour with all three methods. Although we do not present here a detailed investigation of the numerical properties of these schemes, we should report that the original Galloway and Frisch [6] scheme involves a smaller amount of memory requirement and a larger CFL condition.

For all the above schemes, the computing time obviously varies with the control parameter Rm. If all spatial modes are computed up to a truncation N, the computational complexity scales like $\mathcal{O}(N^4)$. Assuming the asymptotic scaling of the magnetic field length scale, we get $N \sim \mathrm{Rm}^{1/2}$ and thus expect a complexity growing as $\mathcal{O}(\mathrm{Rm}^2)$. We have therefore derived a parallel version of the code using the MPI library and a spectral domain decomposition strategy to tackle larger values of Rm. This yields shorter computing time at large resolution.

The results presented in this article were obtained with numerical resolutions ranging from $N = 64$ for the smallest values of Rm to $N = 1024$ for $\mathrm{Rm} = 25000$. In all cases we verified that the results reported here were unaltered by doubling the resolution. The simulations presented here were performed on up to 512 cores.

It is worth stressing that the quantity $\boldsymbol{\nabla} \cdot \mathbf{B}$ is obviously preserved by (1), and that this essential property is retained by the discrete numerical schemes, and thus the magnetic field remains solenoidal throughout the simulations.

We investigate a linear problem and therefore expect that, independently of the initial conditions, the long time integration will simply reflect the eigenmode with largest growth rate. In practice, we used two different sets of initial conditions, either

$$\mathbf{B}(t=0) \propto (\sin z - \cos y)\,\mathbf{e}_x + (\sin x - \cos z)\,\mathbf{e}_y + (\sin y - \cos x)\,\mathbf{e}_z\,, \tag{6}$$

or a random initial condition with a spectrum converging as $\mathbf{k}^{-2}$ for regularity and projected numerically to get a non-divergent field.

The former is useful for comparison with earlier studies (e.g. Galloway and Frisch [6]) for moderate values of Rm, while the later ensures a projection of the initial perturbation on

the fastest growing mode.

III. MODES CROSSING

This study is focused on the 1:1:1 ABC-flow, which has a large number of symmetries. These have been well documented[16,17]. The symmetry group is generated by two independent rotations: the cloverleaf rotation $T : x \to y \to z \to x$ and a rotation of angle $\pi/2$ followed by a translation around one of the three coordinate axes. For example $Rt_y : x \to \pi/2 + z, y \to y - \pi/2, z \to \pi/2 - x$. All the other symmetries are obtained by combinations of these two rotations. The resulting group of symmetries of the ABC-flow contains 24 elements (including identity). For each direct numerical simulation, we tested which of these symmetries (or anti-symmetries) were satisfied by the realised solution.

Figure 1 presents the evolution of the maximum growth rate of the magnetic field as a function of Rm. Each point on the figure corresponds to a three-dimensional simulation. We confirm growth rates obtained by earlier studies (see Galloway[12] for a recent review), and we extend the range of investigation from Rm < 1600 to Rm < 25000. The curve has been validated against published growth rates using spectral methods[7,18] as well as a finite volume method[19] for which simulations have been performed up to Rm $= 2000$ (Teyssier & Dormy private comm.).

In addition to the wider extend of Rm variation, our curve also offers a finer resolution than previously obtained graphs. This highlights the presence for two kinks in the curve, labelled Rm_1 and Rm_2 on the figure. The first of these occurs in the stable window reported by Galloway and Frisch[7] near Rm $= 20$ and corresponds to $\mathrm{Rm}_1 \in [24.05, 24.10]$. A mode crossing was previously suggested owing to the changes in the eigenfunction symmetry[12]. Here we demonstrate this eigenvalue crossing by following both eigenvalues on each side of the crossing. In fact whereas time stepping algorithms usually only provide information on the dominant eigenvalue, i.e. the eigenmode with largest growth rate, we use it here to get more information. Indeed, transient behaviour starting with well selected initial conditions provide information on the behaviour of a given mode, even if it is not the dominant eigenmode (see Figure 2). The temporal behaviour of this mode can be followed via direct integration for a certain length of time until it is overcome by the fastest growing mode. This approach allowed us to continue the branches corresponding to each eigenvalue

FIG. 1. Plot of the real part of the eigenvalue for the fastest growing magnetic field mode as a function of the magnetic Reynolds number Rm (using logarithmic scale in the x-axis).

a. b.

FIG. 2. Time evolution of the magnetic energy, which highlights the information provided by transient behaviours. Left (a) a simulation for $\mathrm{Rm} = 16.5\,(< \mathrm{Rm}_1)$ using as initial condition the final solution obtained at $\mathrm{Rm} > \mathrm{Rm}_1$, right (b) simulation for $\mathrm{Rm} = 28.4\,(> \mathrm{Rm}_1)$.

outside of the region in which they are dominant eigenvalues (see dotted lines and open symbols on Figure 1).

In the first window $\mathrm{Rm} < \mathrm{Rm}_1$ as argued by Arnol'd[16], we observe that the dominant eigenmode has all "even" symmetries of the ABC-flow, i.e. it has every combination of an even number of Rt as a symmetry, and is antisymmetric otherwise (the solution changes

sign by the corresponding transformation). In the second window $\mathrm{Rm} > \mathrm{Rm}_1$, we observe numerically that all the above symmetries and anti-symmetries disappear, as pointed by Galloway and Frisch[7]. However, S. Jones and A. Gilbert (private comm.) are currently using a decomposition of this mode in three components each satisfying different symmetries.

As noted by earlier authors, the dominant eigenvalues are complex, leading to oscillations of the energy, visible on Figure 2 (particularly on the first part of Figure 2a, as the period of oscillations is elsewhere very short compared to the time extend of the plot). The imaginary part of the dominant eigenvalue $\omega = \mathrm{Im}\,(\lambda)$ can thus be directly determined from these time series. The graph $\omega(\mathrm{Rm})$ is displayed on Figure 3. As explained above, not only do we display the dominant eigenvalue (solid line and symbols) but we are also able to follow each mode past their region of selection (dotted lines and open symbols). One can note that, as Rm increases past Rm_1, the imaginary part of the dominant eigenvalue jumps discontinuously from $\omega \simeq 0.53$, corresponding to the first window identified by Arnold and Korkina[5], to $\omega \simeq 0.13$ corresponding to the second window of Galloway and Frisch[7]. This discontinuous jump in the pulsation highlights the eigenvalue crossing occurring at Rm_1. There again, transient behaviours were used to obtain the open symbols.

IV. OSCILLATORY DYNAMICS

In order to obtain a deeper understanding of the oscillatory mechanism in both dynamo windows and of how a steadily growing mode can be observed at larger Rm (see Figure 3), we introduce a phase space for this linear system. We rely for $\mathrm{Rm} < \mathrm{Rm}_1$ on two vectors, corresponding respectively to the dominant $|\mathbf{k}| = 1$ contribution[16]

$$\mathbf{b}_1 = (\sin(z) - \cos(y))\,\mathbf{e}_x + (\sin(x) - \cos(z))\,\mathbf{e}_y + (\sin(y) - \cos(x))\,\mathbf{e}_z\,, \tag{7}$$

and to $|\mathbf{k}| = 2$

$$\mathbf{b}_2 = (\sin(y)\cos(z))\,\mathbf{e}_x + (\sin(z)\cos(x))\,\mathbf{e}_y + (\sin(x)\cos(y))\,\mathbf{e}_z\,. \tag{8}$$

These vector fields respectively correspond to the first and the second harmonics of the true eigenvector. These two vector fields necessarily satisfy all symmetries of the realised eigenmode for this parameter regime ($\mathrm{Rm} < \mathrm{Rm}_1$).

Simulations in this regime rapidly reach an asymptotic behaviour starting with $\mathbf{b}_1$ as an initial condition.

FIG. 3. Plot of the imaginary part of the eigenvalue as a function of Rm (using logarithmic scale in the x-axis).

We construct the phases by introducing

$$X = \langle \mathbf{B} \cdot \mathbf{b}_1 \rangle \exp^{-\sigma t}, \quad \text{and} \quad Y = \langle \mathbf{B} \cdot \mathbf{b}_2 \rangle \exp^{-\sigma t}, \tag{9}$$

where the growth rate σ is a function of Rm (see figure 1). As the governing equations are linear, the exponential damping is here essential in order to introduce a limit behaviour. The quantities X and Y are presented on figure 4a for Rm = 11.5. The undamped trajectory of the system is also represented using dashed lines, and directly illustrates the exponential growth of the dominant mode. The damped trajectory evolves toward the equivalent of a stable limit cycle.

The exponential damping on X and Y provides us with the equivalent of a non-linear dynamical system. This explains why we report below phenomena that are usually associated to non-linear dynamics.

In the second window, Rm $>$ Rm_1, the two modes we selected (corresponding to the

a. b.

FIG. 4. Phase space diagrams for $\mathrm{Rm} < \mathrm{Rm}_1$ (a) and $\mathrm{Rm} > \mathrm{Rm}_1$ (b).

lowest $\vec{k}$ component of the realised mode) are

$$\mathbf{b}'_1 = (-\sin(y) - \cos(z))\,\mathbf{e}_x + (\sin(z) + \cos(x))\,\mathbf{e}_y + (-\sin(x) + \cos(y))\,\mathbf{e}_z\,, \tag{10}$$

$$\mathbf{b}'_2 = (\sin(y) - \cos(z))\,\mathbf{e}_x + (\sin(z) - \cos(x))\,\mathbf{e}_y + (\sin(x) - \cos(y))\,\mathbf{e}_z\,. \tag{11}$$

These correspond to two components of the general family reported earlier for this mode[7]. Note that these two vectors do not provide a complete decomposition of the first harmonic. They involve symmetries (though none in common), but these are not relevant here since they are not verified by the full eigenmode nor the first harmonic.

The resulting orbits of $X' = \langle \mathbf{B} \cdot \mathbf{b}'_1 \rangle \exp^{-\sigma t}$ and $Y' = \langle \mathbf{B} \cdot \mathbf{b}'_2 \rangle \exp^{-\sigma t}$ are represented on figure 4b for various values of the controlling parameter $\mathrm{Rm} > \mathrm{Rm}_1$. The represented quantities are not arbitrarily rescaled. Only the exponential damping has been applied, and all cases have been started with the same initial condition (involving random, but divergence free, fluctuations). The oscillating nature of the dynamo for $\mathrm{Rm} < \mathrm{Rm}_2$ is clearly illustrated by the limit cycle. For $\mathrm{Rm} > \mathrm{Rm}_2$ the oscillations disappear and the dynamo mode therefore becomes a fixed point in the $[X', Y']$ plan. For clarity, we suppressed the trajectories that lead to the limit cycles or the steady solutions on figure 4b.

V. EIGENVALUES COALESCENCE

As the magnetic Reynolds number is further increased, a second kink in the growth rate is observed on Figure 1 for $\mathrm{Rm}_2 \in [215.0, 215.4]$. This second kink, however, does not correspond to a change of dominant eigenvalue, but instead to an eigenvalues coalescence. The strategy highlighted above to follow secondary modes does not yield any secondary

branch here, indicating that there is no significant change in the dominant eigenmode.

Figure 3 reveals that the behaviour of the imaginary part of the eigenvalue is very different near the second kink. Instead of the abrupt jump reported at Rm_1, the pulsation continuously (but not smoothly) tends to zero as Rm approaches Rm_2 and vanishes for $\mathrm{Rm} > \mathrm{Rm}_2$.

The lack of oscillations at large Rm is a well known characteristic, it was already noticed by Galloway and Frisch [6] for ($\mathrm{Rm} > 400$), although they could not assess whether the period of oscillations was simply increasing with Rm or the eigenvalue had become purely real. Lau and Finn [18] suggested that this could be associated with a mode crossing, a new mode with purely real eigenvalue taking over above Rm_2.

We show here that the imaginary part of the eigenvalue indeed vanishes for $\mathrm{Rm} > \mathrm{Rm}_2$, and that this corresponds to the coalescence of two complex conjugate eigenvalues on the real axis. The coalescence yields the kink in the evolution of the real part of the eigenvalue.

The simplest mathematical model for a complex conjugate eigenvalue coalescence on the real axis corresponds to a situation of the form

$$\lambda_\pm = \alpha(\mathrm{Rm}) \pm \sqrt{\beta(\mathrm{Rm})}\,, \tag{12}$$

where α and β are differentiable real functions of Rm. A negative β (for $\mathrm{Rm} < \mathrm{Rm}_2$) yields two complex conjugate modes, and thus oscillations of the magnetic energy. As β becomes positive (for $\mathrm{Rm} > \mathrm{Rm}_2$), the eigenvalues are purely real and the β term now contributes to the real part of the eigenvalue λ_+ offering the largest growth rate.

Figure 5a presents a detailed view on the variation of $\sigma = \mathrm{Re}\,(\lambda)$ and $\omega = \mathrm{Im}\,(\lambda)$ close to Rm_2. Defining $\sigma_2 = \sigma(\mathrm{Rm}_2)$ we plot $\sigma(\mathrm{Rm}) - \sigma_2$ and $-\omega(\mathrm{Rm})$. It is clear that the kink in σ is concomitant of the vanishing of ω.

Let us now form on Figure 5b the quantity $F = \sigma(\mathrm{Rm}) - \sigma_2 - \omega(\mathrm{Rm})$. The square-root behaviour of F near Rm_2 is obvious. Assuming that the above model (12) is correct, F corresponds to $\alpha - \alpha_0 + \mathrm{sign}\,(\beta)\sqrt{|\beta|}$, where $\alpha_0 = \alpha(\mathrm{Rm}_2)$. We can note on Figure 5a for $\mathrm{Rm} < \mathrm{Rm}_2$ that $\alpha - \alpha_0$ remains small compared to variations in β. The quantity $\mathrm{sign}\,(\mathrm{Rm} - \mathrm{Rm}_2)\,F^2$ therefore offers a good approximation to β and should be differentiable at Rm_2.

More formally, assuming that α and β are regular functions of Rm, we can write a finite

a. b.

FIG. 5. Eigenvalues coalescence for Rm close to $\mathrm{Rm}_2 \simeq 215$. Both the real part (written as $\sigma(\mathrm{Rm}) - \sigma_2$) and the opposite of the imaginary part (i.e. $-\omega(\mathrm{Rm})$) are represented (a). The sum F of both (b), and $\mathrm{sign}\,(\mathrm{Rm} - \mathrm{Rm}_2)F^2$ illustrate the continuity and regularity in the functional form of the eigenvalue (see text).

expansion of the form

$$\alpha = \alpha_0 + \alpha_1(\mathrm{Rm} - \mathrm{Rm}_2) + \alpha_2(\mathrm{Rm} - \mathrm{Rm}_2)^2 + \cdots , \tag{13}$$

$$\beta = \beta_1(\mathrm{Rm} - \mathrm{Rm}_2) + \beta_2(\mathrm{Rm} - \mathrm{Rm}_2)^2 + \cdots , \tag{14}$$

with $\beta_1 > 0$. The quantity $\mathrm{sign}\,(\mathrm{Rm} - \mathrm{Rm}_2)\,F^2$ can be written at the lowest orders in $\mathrm{Rm} - \mathrm{Rm}_2$

$$\begin{aligned} \mathrm{sign}\,(\mathrm{Rm} - \mathrm{Rm}_2)\,F^2 = {} & \mathrm{sign}\,(\mathrm{Rm} - \mathrm{Rm}_2)\alpha_1^2(\mathrm{Rm} - \mathrm{Rm}_2)^2 \\ & + \mathrm{sign}\,(\mathrm{Rm} - \mathrm{Rm}_2)\alpha_1\sqrt{\beta}_1(|\mathrm{Rm} - \mathrm{Rm}_2|)^{3/2} \\ & + \beta_1(\mathrm{Rm} - \mathrm{Rm}_2). \end{aligned} \tag{15}$$

This development implies that $\mathrm{sign}\,(\mathrm{Rm}-\mathrm{Rm}_2)\,F^2$ is differentiable at Rm_2. Figure 5b clearly illustrate this property on the direct numerical simulation.

Another insight on the nature of this transition can be gained from the "phase space" introduced in figure 4b. As noted above a remarkable feature is that the steady solutions obtained after the coalescence lies on the ellipse described by the limit cycle shortly below the coalescence (on the figure Rm = 220). This behaviour which is similar to that of an excitable system (such as a pendulum subject to a constant torque), has recently been observed in experimental dynamos measurements[20]. The phase space was then constructed using two components of the magnetic field at a given location (a probe).

Such behaviour is reminiscent of a saddle-node bifurcation. In these systems, the dynamics becomes increasingly slow on the cycle as the system approaches the state at which

FIG. 6. Evolution in time of the projection of the dominant mode on the two large scale components, represented via the angle θ, such that $(\cos(\theta), \sin(\theta)) = (X', Y')/\sqrt{X'^2 + Y'^2}$.

the saddle and the node will collapse. In order to assess this property in our system, albeit linear, we introduce the angle θ of the system over a unit circle described through the orbit, so that $(\cos(\theta), \sin(\theta)) = (X', Y')/\sqrt{X'^2 + Y'^2}$. The time evolution of θ with increasing values of Rm is presented in figure 6. The system clearly spends an increasing amount of time as Rm approaches Rm_2 near the angle at which the stable solution will occur for $\mathrm{Rm} = \mathrm{Rm}_2$. Such behaviour could be described by a simple phase dynamics, e.g. Pétrélis *et al.*[21], Guckenheimer and Holmes[22].

It is interesting that these approaches of non-linear dynamics can cast some light on the behaviour of kinematic dynamos. A similar occurrence of a saddle-node transition for a kinematic dynamo numerical model of the above mentioned VKS experiment has indeed been reported in Gissinger[23], with an expression of the form (12).

The fact that the fixed points in the (X', Y') plan describe the previously existing limit cycle is a strong indication that there is at first no significant change occurring in the structure of the dominant eigenmode after the eigenvalues coalescence. Indeed the "double cigars" structure (see Dorch[24]), associated to the oscillations for $\mathrm{Rm} \in [\mathrm{Rm}_1, \mathrm{Rm}_2]$ is preserved once the growth rate has become steady, $\mathrm{Rm} > \mathrm{Rm}_2$ (see Figure 7).

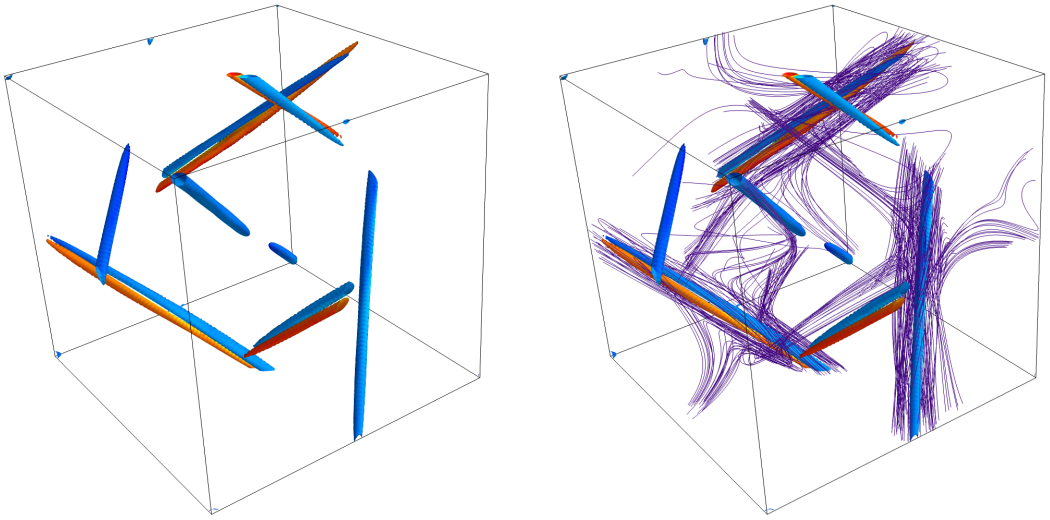

FIG. 7. Eigenmode obtained for Rm = 434.2 ($> \mathrm{Rm}_2$). An isosurface of the magnetic energy is represented. To highlight the symmetry, it is coloured according to the value of B_x, from negative (dark gray - blue online) to positive (lighter gray - red online). The corresponding eigenvalue is purely real, yet the double cigars structure of the field remains clearly visible. Magnetic field lines are also depicted on the right plot.

VI. ASYMPTOTIC BEHAVIOUR

We have finally increased the control parameter in the range 215–25000. Despite the fact that the largest magnetic Reynolds number tackled in this study is roughly 15 times larger than earlier results, the growth rate has not reached an asymptotic value yet. The growth rate obtained for our largest Rm is very close to 0.1 and appears to be still significantly increasing with Rm.

The 1:1:1 ABC-flow has also been considered by Gilbert [25] using maps in a limit in which the diffusivity is formally set to zero. This approach has yield growth rate of 0.04 – 0.05, so much smaller than the value achieved by our direct numerical simulations at Rm = 25000. It is therefore not unplausible to anticipate that the behaviour of $\sigma(\mathrm{Rm})$ above 25000 will not be monotonic and σ will probably decrease again.

Another indication is provided by the largest Lyapunov exponent of the flow, which is approximately 0.055 (see Galanti, Sulem, and Pouquet [26]). Owing to the lack of regularity of the field in the limit of large Rm numbers, the largest Lyapunov exponent however does not provide an upper bound on the asymptotic growth rate[3]. An upper bound can be

sought by considering the topological entropy $h_{\rm top}$ (see Finn and Ott [27,28]). For steady three-dimensional flows the topological entropy is equal to the line stretching exponent $h_{\rm line}$ (see Childress and Gilbert [3]), which can be estimated for the $1:1:1$ ABC-flow to be $h_{\rm line} \simeq 0.09$. This provides yet another indication that the curve $\sigma(\mathrm{Rm})$ must decrease for larger values of Rm.

A plausible scenario, suggested by the behaviour of submodes as investigated by S. Jones and A. Gilbert, is that two complex conjugate eigenvalues may emerge again at larger Rm. This is often observed in saddle-node bifurcations (e.g. Ravelet *et al.* [20]). It would result in the reappearance of the oscillations, and an abrupt decrease of the growth rate (the counterpart of the increase observed at Rm_2). This would deserve further study.

The asymptotic behaviour of the $1:1:1$ ABC-flow is thus not yet established. It is at the moment, despite the high resolution simulations presented here, impossible to assess its asymptotic growth rate. It is not even possible to rule out the possibility of an eventual decay of the growth rate to zero at very large Rm.

VII. CONCLUSION

We have investigated using high resolution direct numerical simulations the behaviour of the $1:1:1$ ABC-dynamo. We have shown that the two dynamo windows identified for this dynamo are associated with a change of dominant eigenvalue. We have identified a second kink in the growth rate as a function of Rm and shown that it corresponds to an eigenvalue coalescence and the end of the oscillatory nature of the solutions. Finally, even at very large values of Rm, we show that the growth rate is still strongly varying and not monotonic yet.

Relaxing the requirement of a fully three-dimensional flow and allowing for time dependence, other models for fast dynamo actions have been obtained by Galloway and Proctor [29], with a velocity depending only on two coordinates. The time dependence ensures exponential stretching at least in this plane. The induction equation is then separable in the z direction, allowing faster numerical integrations. The asymptotic limit of large Rm appears easier to reach for such flows. Other studies involved time dependence of the flow[30] and some hint at a possible resonance phenomenon[31].

Finding a good example of fully three-dimensional flow that acts as a fast dynamo remains a challenging problem. The most classically given example remains the $1:1:1$ ABC-flow.

This unexpectedly rich behaviour of the 1:1:1 ABC-dynamo at very large Rm, highlighted in our study, deserves further investigations. It is most likely associated with the fact this flow yields very small chaotic regions[12].

ACKNOWLEDGEMENTS

The authors are very grateful to Dave Galloway for sharing his original dynamo code, which served as the starting point for the parallel version written for this study. We are also very grateful to Christophe Gissinger for useful discussions in the course of this work. Computations were performed on the MesoPSL cluster as well as on the Cines computing centre (Genci project LRA0633).

REFERENCES

[1]T. Dombre, U. Frisch, J. Greene, M. Henon, A. Mehr, and A. Soward, "Chaotic streamlines in the ABC flows," J. Fluid Mech **167**, 353–391 (1986).

[2]V. Arnol'd, Y. Zel'dovich, A. Ruzmaikin, and D. Sokolov, "Magnetic field in a stationary flow with stretching in riemannian space," Sov. Phys.-JETP (Engl. Transl.);(United States) **54** (1981).

[3]S. Childress and A. Gilbert, *Stretch, twist, fold: the fast dynamo* (Springer-Verlag Berlin and Heidelberg, 1995).

[4]M. M. Vishik, "Magnetic field generation by the motion of a highly conducting fluid," Geophysical & Astrophysical Fluid Dynamics **48**, 151–167 (1989).

[5]V. Arnold and E. Korkina, "The growth of a magnetic field in the three-dimensional steady flow of an incompressible fluid," Moskovskii Universitet Vestnik Seriia Matematika Mekhanika **1**, 43–46 (1983).

[6]D. Galloway and U. Frisch, "A numerical investigation of magnetic field generation in a flow with chaotic streamlines," Geophysical & Astrophysical Fluid Dynamics **29**, 13–18 (1984).

[7]D. Galloway and U. Frisch, "Dynamo action in a family of flows with chaotic streamlines," Geophysical & Astrophysical Fluid Dynamics **36**, 53–83 (1986).

[8]D. Galloway and U. Frisch, "A note on the stability of a family of space-periodic beltrami flows," Journal of Fluid Mechanics **180**, 557–564 (1987).

[9]A. Courvoisier, A. Gilbert, and Y. Ponty, "Dynamo action in flows with cat's eyes," Geophysical and Astrophysical Fluid Dynamics **99**, 413–429 (2005).

[10]V. Archontis, S. Dorch, and Å. Nordlund, "Nonlinear mhd dynamo operating at equipartition," Astronomy and Astrophysics **472**, 715–726 (2007).

[11]A. Alexakis, "Searching for the fastest dynamo: Laminar ABC flows," Physical Review E **84**, 026321 (2011).

[12]D. Galloway, "Abc flows then and now," Geophysical & Astrophysical Fluid Dynamics **106**, 450–467 (2012).

[13]V. Arnold, "Sur la topologie des écoulements stationnaires des fluides parfaits," CR Acad. Sci. Paris **261**, 17–20 (1965).

[14]M. Henon, "Sur la topologie des lignes de courant dans un cas particulier," CR Acad. Sci. Paris **262**, 312–314 (1966).

[15]V. Archontis, S. Dorch, and Å. Nordlund, "Numerical simulations of kinematic dynamo action," Astronomy and Astrophysics **397**, 393–399 (2003).

[16]V. Arnol'd, "On the evolution of a magnetic field under the action of transport and diffusion," Amer. Math. Soc. Transl. **137**, 119–129 (1987).

[17]O. Podvigina, "Spatially-periodic steady solutions to the three-dimensional navier-stokes equation with the abc-force," Physica-Section D **128**, 250–272 (1999).

[18]Y. Lau and J. Finn, "Fast dynamos with finite resistivity in steady flows with stagnation points," Physics of Fluids B: Plasma Physics **5**, 365 (1993).

[19]R. Teyssier, S. Fromang, and E. Dormy, "Kinematic dynamos using constrained transport with high order godunov schemes and adaptive mesh refinement," Journal of Computational Physics **218**, 44–67 (2006).

[20]F. Ravelet, M. Berhanu, R. Monchaux, S. Aumaître, A. Chiffaudel, F. Daviaud, B. Dubrulle, M. Bourgoin, P. Odier, J.-F. Pinton, N. Plihon, R. Volk, S. Fauve, N. Mordant, and F. Pétrélis, "Chaotic dynamos generated by a turbulent flow of liquid sodium," Physical review letters **101**, 74502 (2008).

[21]F. Pétrélis, S. Fauve, E. Dormy, and J. Valet, "Simple mechanism for reversals of earth's magnetic field," Physical review letters **102**, 144503 (2009).

[22]J. Guckenheimer and P. Holmes, *Nonlinear oscillations, dynamical systems, and bifurcations of vector fields*, Vol. 42 (Springer-Verlag New-York, 1997).

[23]C. Gissinger, "A numerical model of the vks experiment," EPL (Europhysics Letters) **87**, 39002 (2009).

[24]S. Dorch, "On the structure of the magnetic field in a kinematic ABC flow dynamo," Physica Scripta **61**, 717 (2000).

[25]A. Gilbert, "Magnetic field evolution in steady chaotic flows," Philosophical Transactions of the Royal Society of London. Series A: Physical and Engineering Sciences **339**, 627–656 (1992).

[26]B. Galanti, P. Sulem, and A. Pouquet, "Linear and non-linear dynamos associated with ABC flows," Geophysical & Astrophysical Fluid Dynamics **66**, 183–208 (1992).

[27]J. Finn and E. Ott, "Chaotic flows and fast magnetic dynamos," Physics of Fluids **31**, 2992 (1988).

[28]J. Finn and E. Ott, "Chaotic flows and magnetic dynamos," Physical review letters **60**, 760–763 (1988).

[29]D. Galloway and M. Proctor, "Numerical calculations of fast dynamos in smooth velocity fields with realistic diffusion," Nature **356**, 691–693 (1992).

[30]N. Otani, "A fast kinematic dynamo in two-dimensional time-dependent flows," Journal of Fluid Mechanics **253**, 327–340 (1993).

[31]E. Dormy and D. Gerard-Varet, "Time scales separation for dynamo action," EPL (Europhysics Letters) **81**, 64002 (2008).